CHARACTERISTICS AND STRUCTURES OF TURBULENT BOUNDARY LAYER WITH COUNTER DIFFUSION GRADIENT PHENOMENON

H. Hattori, K. Hotta, T. Houra and M. Tagawa
Department of Mechanical Engineering
Nagoya Institute of Technology
Gokiso-cho, Showa-ku, Nagoya 466-855, JAPAN
hattori@nitech.ac.jp

ABSTRACT

The objectives of this study are to investigate a counter diffusion phenomenon (CDP) in a stably thermally-stratified turbulent boundary layer by means of direct numerical simulation (DNS). In this study, four cases of stably thermally-stratified turbulent boundary layer are simulated in order to reproduce the CDP, in which two Reynolds numbers and four Richardson numbers are set. The CPD is discovered in both the velocity and thermal fields in three cases. DNS clearly shows the CDP which indicates the negative sign of the Reynolds shear stress and the wall-normal turbulent heat flux with the positive sign of mean velocity and temperature gradients. In the case of strong occurrence of CDP, the local Richardson number always exceeds the critical Richardson number, but the turbulence is maintained. Also, the anisotropy tensor and invariant map are indicated in this paper. It is found that the state of turbulent stress rapidly arrives in the axisymmetric in the case of occurrence of CDP. The turbulent heat flux tensor is also shown in order to indicate the variation of thermal field, in which the streamwise turbulent heat flux tensor maintains high value even in the case of strong occurrence of CDP. The relation between the vortex structure and the fluctuation of Reynolds shear stress is shown, where the negative value of fluctuation of Reynolds shear stress frequently appears around the vortex structure in the case of occurrence of CDP.

INTRODUCTION

Thermally-stratified turbulent boundary layer has been often encountered in the real fluid flow, and it is very important to know the characteristics and structure of such a flow for satisfying our probing intellectual curiosity. Thus, in order to investigate and observe thermally-stratified turbulent boundary layer in detail, the direct numerical simulation (DNS) has been carried out (Hattori *et al.*, 2007; Hattori & Nagano, 2007; Hattori *et al.*, 2012). In the previous study (Hattori & Nagano, 2007; Hattori *et al.*, 2012), a counter gradient diffusion phenomenon (CDP) is observed in a stably thermally-stratified turbulent boundary layer in both the velocity and thermal fields. In a stably thermally-stratified turbulent boundary layer (Komori & Nagata, 1996; Ohya, 2001), a non-premixed turbulent flame formed in a strong pressure-gradient flow (Tagawa *et al.*, 2005), a turbulent boundary layer with separation and reattachment (Hattori & Nagano, 2012; Hattori *et al.*, 2013), etc., a CDP is sometimes observed contrary to the principle of gradient diffusion. Reynolds shear stress or turbulent heat flux are modeled using the relation of conventional gradient diffusion hypothesis with the eddy diffusivity, e.g., $-\overline{uv} = \nu_t(\partial \bar{U}/\partial y)$ for a velocity field. Thus, the eddy diffusivity indicates negative value, if a CDP occurs. A CDP suppresses obviously the transport phenomena in turbulence due to the negative value of the eddy diffusivity. In order to cause a CDP, the extra force such a strong thermal stratification is needed. However, the criterion for an occurrence of CDP is inarticulate. Therefore, the objectives of this study are to explore a causation of occurrence of CDP, and to investigate it in stably thermally-stratified turbulent boundary layer by means of DNS in detail. In particular, it has been discovered in the previous study that CDP occurs in a high Richardson number of stable stratification, but a stably thermally-stratified turbulent boundary layer has never been explored as for variation of Reynolds numbers. Thus, DNSs have been conducted under various Reynolds and Richardson numbers conditions so as to detect the criterion for occurrence of CDP. Also, the detailed turbulent statistics and structures such as the anisotropy invariant of turbulence in the stably thermally-stratified turbulent boundary layers are revealed to understand the turbulent characteristics of such a flow field.

DNS OF STABLY THERMALLY-STRATIFIED BOUNDARY LAYER

Assuming that the Boussinesq approximation is approved for the Navier-Stokes equation, the governing equations used in the present DNS are indicated as follows (Hattori *et al.*, 2007):

$$\frac{\partial u_i^*}{\partial x_i^*} = 0 \tag{1}$$

$$\frac{Du_i^*}{Dt} = -\frac{\partial p^*}{\partial x_i^*} + \frac{1}{Re_{\delta_{2,\mathrm{in}}}}\frac{\partial^2 u_i^*}{\partial x_j^* \partial x_j^*} + \delta_{i2} Ri_{\delta_{2,\mathrm{in}}} \theta^* \tag{2}$$

$$\frac{D\theta^*}{Dt} = \frac{1}{PrRe_{\delta_{2,\mathrm{in}}}}\frac{\partial^2 \theta^*}{\partial x_j^* \partial x_j^*} \tag{3}$$

where the Einstein summation convention applies to repeated indices, and u_i^* is the dimensionless velocity component in x_i direction, θ^* is the dimensionless temperature

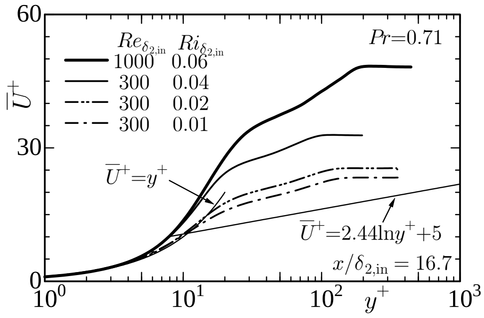

(a) Streamwise mean velocity

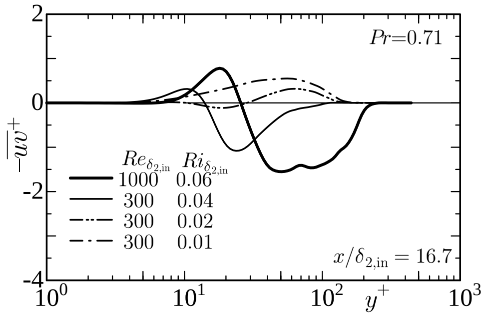

(b) Reynolds shear stress

Figure 1. Profiles of mean velocity and Reynolds shear stress

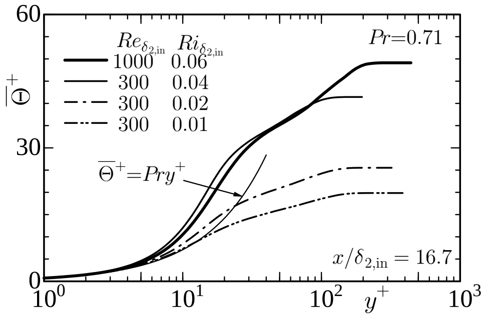

(a) Mean temperature

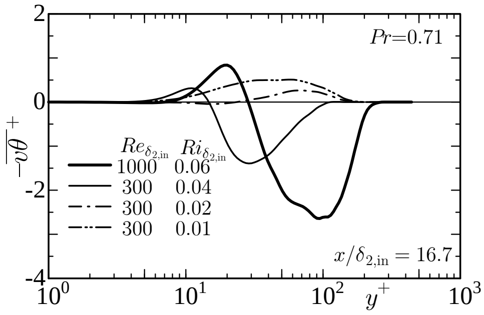

(b) Wall-normal turbulent heat flux

Figure 2. Profiles of mean temperature and turbulent heat flux

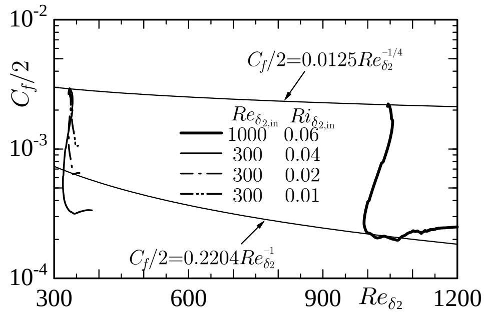

(a) Friction coefficient

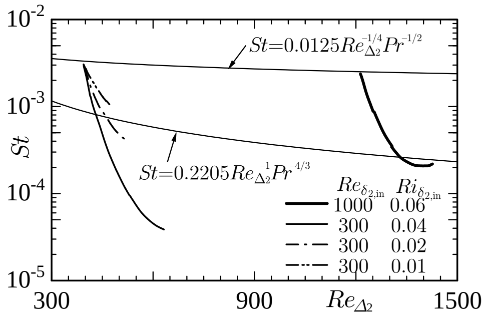

(b) Stanton number

Figure 3. Friction coefficients and Stanton numbers

difference, p^* is the dimensionless pressure, t^* is the dimensionless time, and x_i^* is the dimensionless spatial coordinate in the i direction, respectively. $Re_{\delta_{2,\mathrm{in}}} = U_0\delta_{2,\mathrm{in}}/\nu$ is the Reynolds number based on the free stream velocity and the momentum thickness at the inlet of the driver part, $\delta_{2,\mathrm{in}}$. Note that "the driver part" means the inflow data generator for the inlet boundary of the main simulation part (Hattori *et al.*, 2007). $Pr = \nu/\alpha$ is the Prandtl number, and $Ri_{\delta_{2,\mathrm{in}}} = g\beta\delta_{2,\mathrm{in}}\Delta\Theta/U_0^2$ is the bulk Richardson number based on the free stream velocity, the momentum thickness at the inlet of the driver part, and the temperature difference between a free stream and a wall ($\Delta\Theta = \bar{\Theta}_0 - \bar{\Theta}_w$). In the governing equations, the dimensionless variables are given using the free stream velocity, U_0, and the free stream temperature, Θ_0, at the inlet of the driver part, and the wall temperature, Θ_w.

For efficiently conducting the DNS of thermal boundary layers, the computational domain is composed of two parts; one is the driver part where a zero-pressure-gradient (ZPG) flow with an isothermal wall is generated and used as the inflow boundary condition for the main simulation, and the other is the main part where stable thermal boundary layer flows are simulated. A central finite-difference method of second-order accuracy is used to solve the equations of continuity, momentum and energy (Hattori & Nagano, 2004), where $x \times y \times z = 384 \times 128 \times 128$ of grid points are used for the main part. Although thirty times the momentum thickness at the inlet of the driver part region (about three times of the 99% boundary layer thickness) for wall-normal direction is set, the 70% grid points are distributed in the turbulent boundary layer. The Prandtl number is set to 0.71, assuming the working fluid to be air. The Reynolds numbers are set to 1000 and 300, and the Richardson numbers are set to 0.01 and 0.06 ($Re_{\delta_{2,\mathrm{in}}} = 1000$), 0.01, 0.02 and 0.04 ($Re_{\delta_{2,\mathrm{in}}} = 300$). The non-slip condition for the wall and the convective boundary condition is used at the outlet are adopted for the velocity field. For the thermal field, the isothermal condition for the wall and ambient, where a cooled wall is set for stable flow, i.e., $\Theta_w < \Theta_0$. The convective boundary condition at the outlet is adopted. For the spanwise direction, the periodic condition is adopted for both the velocity and the thermal fields.

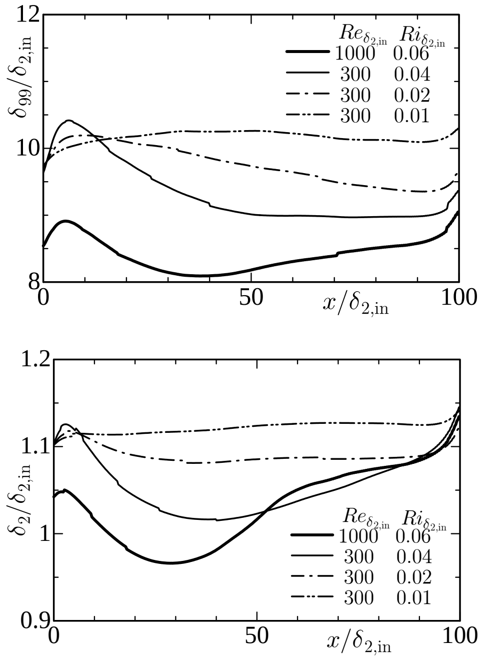

(a) Velocity field

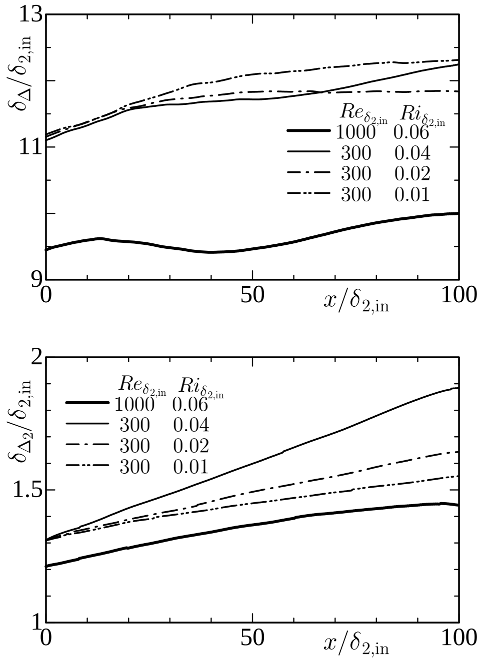

(b) Thermal field

Figure 4. Boundary layer thicknesses

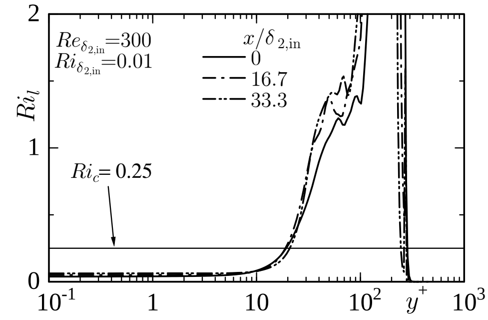

(a)$Re_{\delta_{2,\mathrm{in}}} = 300, Ri_{\delta_{2,\mathrm{in}}} = 0.01$

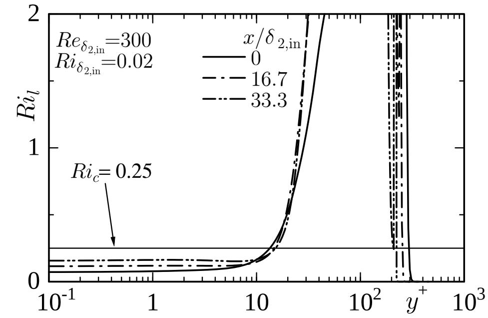

(b) $Re_{\delta_{2,\mathrm{in}}} = 300, Ri_{\delta_{2,\mathrm{in}}} = 0.02$

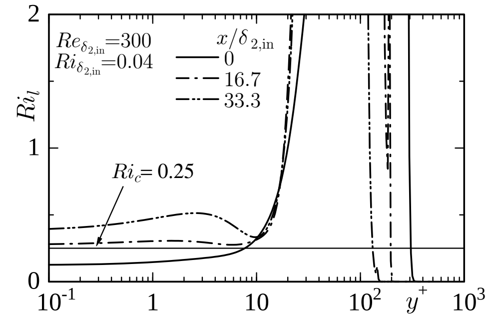

(c) $Re_{\delta_{2,\mathrm{in}}} = 300, Ri_{\delta_{2,\mathrm{in}}} = 0.04$

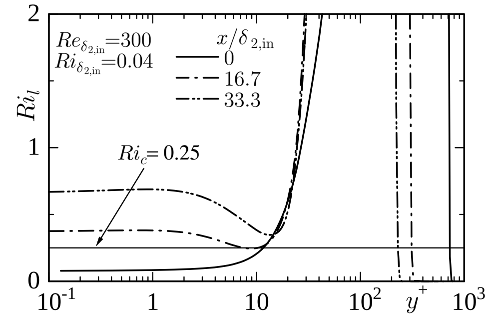

(d) $Re_{\delta_{2,\mathrm{in}}} = 1000, Ri_{\delta_{2,\mathrm{in}}} = 0.06$

Figure 5. Distributions of local Richardson number

RESULTS AND DISCUSSION
Occurrence of CDP

Figure 1 shows profiles of streamwise mean velocity and Reynolds shear stress. The gradients of streamwise mean velocity indicate the positive value in all cases, but it can be seen that the Reynolds shear stresses are shown the negative value in cases of $Re_{\delta_{2,\mathrm{in}}} = 1000$ with $Ri_{\delta_{2,\mathrm{in}}} = 0.06$, and $Re_{\delta_{2,\mathrm{in}}} = 300$ with $Ri_{\delta_{2,\mathrm{in}}} = 0.04, 0.02$, i.e., the occurrence of counter diffusion phenomenon (CDP) is found in the present DNS. In particular, an obvious negative value of Reynolds shear stress can be observed in cases of $Re_{\delta_{2,\mathrm{in}}} = 1000$ with $Ri_{\delta_{2,\mathrm{in}}} = 0.06$, and $Re_{\delta_{2,\mathrm{in}}} = 300$ with $Ri_{\delta_{2,\mathrm{in}}} = 0.04$. On the other hand, mean temperature and wall-normal turbulent heat flux are shown in Fig. 2. In the thermal field, the CDP can be clearly observed in the same cases of velocity field.

The counter gradient diffusion phenomenon is defined as $\nu_t = -\overline{uv}/(\partial \bar{U}/\partial y) < 0$ or $\alpha_t = -\overline{v\theta}/(\partial \bar{\Theta}/\partial y) < 0$, where ν_t is the eddy diffusivity for momentum, and α_t is the eddy diffusivity for heat. On the other hand, since the Grashof number is defined as $Gr_{\delta_{2,\mathrm{in}}} = g\beta\delta_{2,\mathrm{in}}^3 \Delta\Theta/\nu^2 = Ri_{\delta_{2,\mathrm{in}}} Re_{\delta_{2,\mathrm{in}}}^2$, Grashof numbers of each cases are calculated

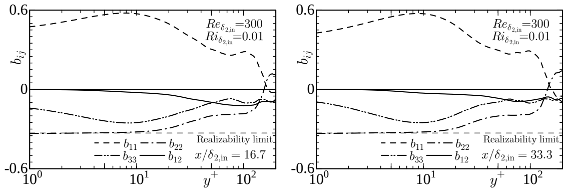

(a) $Re_{\delta_{2,\text{in}}} = 300, Ri_{\delta_{2,\text{in}}} = 0.01$

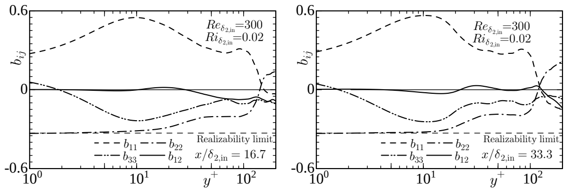

(b) $Re_{\delta_{2,\text{in}}} = 300, Ri_{\delta_{2,\text{in}}} = 0.02$

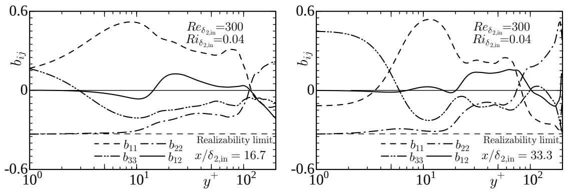

(c) $Re_{\delta_{2,\text{in}}} = 300, Ri_{\delta_{2,\text{in}}} = 0.04$

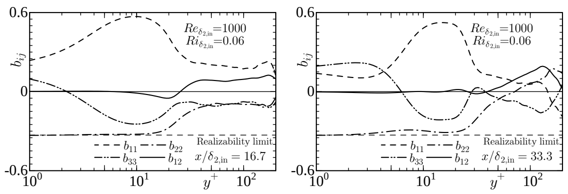

(d) $Re_{\delta_{2,\text{in}}} = 1000, Ri_{\delta_{2,\text{in}}} = 0.06$

Figure 6. Distributions of anisotropy tensor

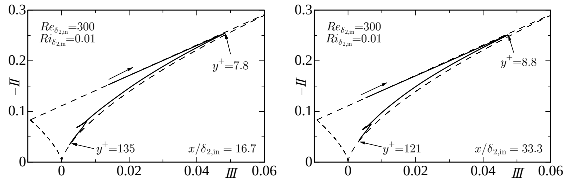

(a) $Re_{\delta_{2,\text{in}}} = 300, Ri_{\delta_{2,\text{in}}} = 0.01$

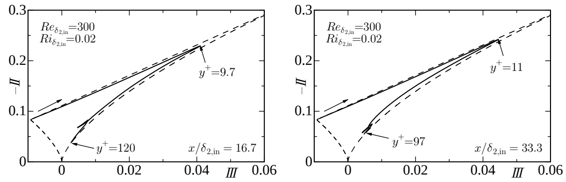

(b) $Re_{\delta_{2,\text{in}}} = 300, Ri_{\delta_{2,\text{in}}} = 0.02$

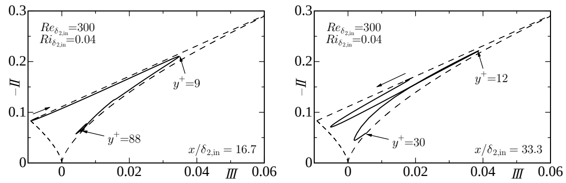

(c) $Re_{\delta_{2,\text{in}}} = 300, Ri_{\delta_{2,\text{in}}} = 0.04$

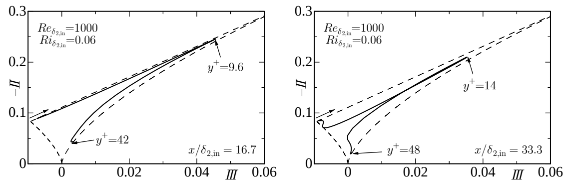

(d) $Re_{\delta_{2,\text{in}}} = 1000, Ri_{\delta_{2,\text{in}}} = 0.06$

Figure 7. Anisotropy invariant maps of Reynolds stress

as 6×10^4 for the case of $Re_{\delta_{2,\text{in}}} = 1000$ with $Ri_{\delta_{2,\text{in}}} = 0.06$ and 3.6×10^3 and 1.8×10^3 for the case of $Re_{\delta_{2,\text{in}}} = 300$ with $Ri_{\delta_{2,\text{in}}} = 0.04, 0.02$, respectively. The Grashof number is 1×10^4 in the case of $Re_{\delta_{2,\text{in}}} = 1000$ with $Ri_{\delta_{2,\text{in}}} = 0.01$ (not shown in the figures), which exceeds the case of low Reynolds number as indicated above, but CDP is not observed. Thus, the Grashof number might not be used for the criterion for occurrence of CDP.

Variations of turbulent parameters

Friction coefficients and Stanton numbers are shown in Fig. 3. In the stably thermally-stratified turbulent boundary layer, it was found that both the friction coefficient and Stanton number decrease (Hattori *et al.*, 2007). In cases of higher Richardson numbers, the friction coefficient and Stanton number remarkably decrease in comparison with lower Richardson number, in which both the friction coefficient and Stanton number are smaller than the values of laminar flow in the case of lower Reynolds number. Figure 4 shows boundary layer thicknesses in both the velocity and thermal fields. The CDP disturbs the transport of momentum or temperature due to decrease of the effective diffusion coefficient (molecular and turbulent diffusion coefficients). Thus, the boundary layer thicknesses of velocity field, δ_{99} and δ_2, obviously decrease while occurrence of CDP. However, it is found that the boundary layer thicknesses of thermal field, δ_t and $\delta_{\Delta 2}$, do not decrease except for the case of $Re_{\delta_{2,\text{in}}} = 300$ with $Ri_{\delta_{2,\text{in}}} = 0.04$.

On the other hand, the local Richardson numbers of all cases are shown in Fig. 5. The local Richardson number is given as follows (Hattori *et al.*, 2007):

$$Ri_l = \frac{g\beta \frac{\partial \bar{\Theta}}{\partial y}}{\left(\frac{\partial \bar{U}}{\partial y}\right)^2} \qquad (4)$$

In cases of $Re_{\delta_{2,\text{in}}} = 1000$ with $Ri_{\delta_{2,\text{in}}} = 0.06$ and $Re_{\delta_{2,\text{in}}} = 300$ with $Ri_{\delta_{2,\text{in}}} = 0.04$ where the CDP occurs outer region, the local Richardson number almost exceeds the critical Richardson number, $Ri_c = 0.025$, near the wall. On the contrary, in the case of $Re_{\delta_{2,\text{in}}} = 300$ with $Ri_{\delta_{2,\text{in}}} = 0.02$, it can be found that the local Richardson number does not exceed the critical Richardson number near the wall. Thus, the CDP occurs near the wall. Thus, the distribution of local Richardson number relates the criterion for strong occurrence of the CDP.

Anisotropy and turbulent heat flux tensors, and turbulent structure in CDP

In order to investigate turbulent state in detail, the anisotropy tensor and map (Simonsen & Krogstad, 2005) are indicated in Figs. 6 and 7, where the anisotropy tensor,

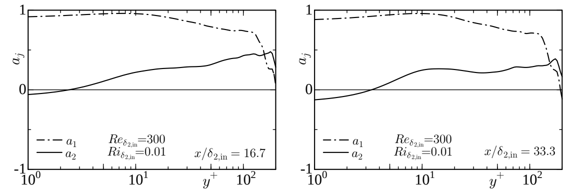

(a) $Re_{\delta_{2,\mathrm{in}}} = 300, Ri_{\delta_{2,\mathrm{in}}} = 0.01$

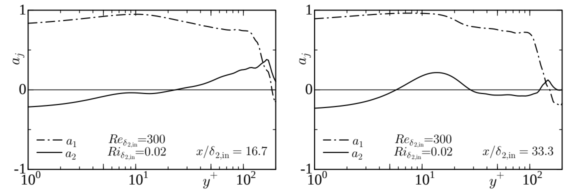

(b) $Re_{\delta_{2,\mathrm{in}}} = 300, Ri_{\delta_{2,\mathrm{in}}} = 0.02$

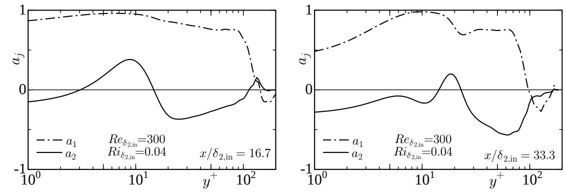

(c) $Re_{\delta_{2,\mathrm{in}}} = 300, Ri_{\delta_{2,\mathrm{in}}} = 0.04$

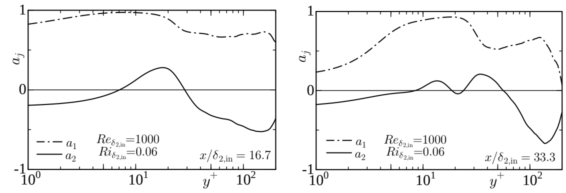

(d) $Re_{\delta_{2,\mathrm{in}}} = 1000, Ri_{\delta_{2,\mathrm{in}}} = 0.06$

Figure 8. Distributions of turbulent heat flux tensor

b_{ij}, is given as follows (Simonsen & Krogstad, 2005):

$$b_{ij} = \frac{\overline{u_i u_j}}{\overline{u_k u_k}} - \frac{1}{3}\delta_{ij} \tag{5}$$

In the case of weak stable stratification, $Re_{\delta_{2,\mathrm{in}}} = 300$ with $Ri_{\delta_{2,\mathrm{in}}} = 0.01$ where the CDP does not appear, the distribution of anisotropy tensor indicates similar distribution of that in the neutrally stratified boundary layer. In other cases, the anisotropy tensors clearly show difference distributions. In particular, the tendency of b_{33} varies near the wall, in which b_{33} indicates the positive value. Also, it can be observed that b_{33} balances b_{12} in the region of occurrence of CDP.

Figure 7 shows the invariant maps for the stably thermally-stratified turbulent boundary layer. In the weak stably thermally-stratified turbulent boundary layer as shown in Fig. 7(a), the invariant moves from the two-component (2C) state to the isotropic (ISO) state via one component (1C) state, but the invariant does not reach at the isotropic state, and it is on the axisymmetric line. The maps of other cases are calculated at the occurrence region of CDP. In the case of remarkable occurrence of CDP as shown in Figs. 7(c) and (d), the anisotropy invariant rapidly goes to the axisymmetric line in comparison with the case of $Re_{\delta_{2,\mathrm{in}}} = 300$ with $Ri_{\delta_{2,\mathrm{in}}} = 0.01$, and the anisotropy invariant does not go to 1C state.

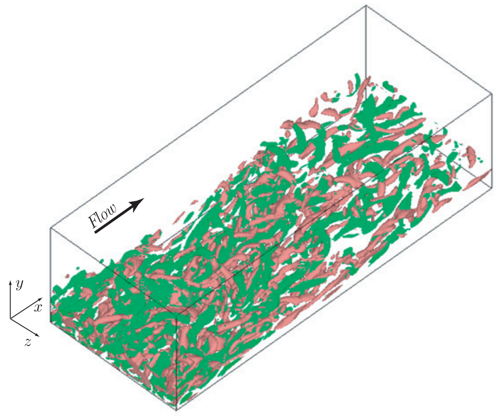

(a)$Re_{\delta_{2,\mathrm{in}}} = 300, Ri_{\delta_{2,\mathrm{in}}} = 0.02$

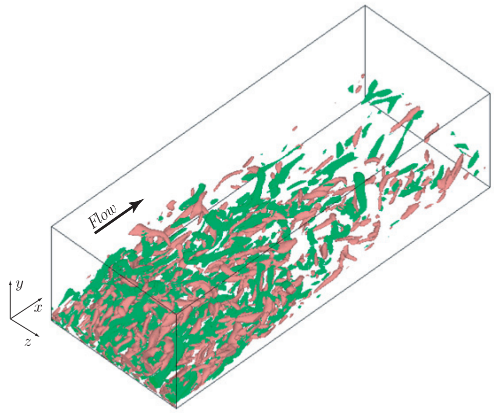

(b) $Re_{\delta_{2,\mathrm{in}}} = 300, Ri_{\delta_{2,\mathrm{in}}} = 0.04$

Figure 9. Variations of vortex structures

As for the thermal field, the following turbulent heat flux tensors are shown in Fig. 9.

$$a_j = \frac{\overline{u_j\theta}}{\sqrt{\overline{u_{(j)}u_{(j)}}}\sqrt{\overline{\theta^2}}} \tag{6}$$

where, the parenthetic index does not apply the Einstein summation convention, i.e., $a_1 = \overline{u_1\theta}/\left(\sqrt{\overline{u_1^2}}\sqrt{\overline{\theta^2}}\right)$ for $j = 1$. In the case of $Re_{\delta_{2,\mathrm{in}}} = 300$ with $Ri_{\delta_{2,\mathrm{in}}} = 0.01$, although the CDP is difficult to find in the foregoing figures, the CDP can be slightly detected close to the wall as shown in Fig. 9(a). In the other cases, it is obvious that the tensor a_1 maintains a near value to 1, but in cases of higher Richardson number, the near-wall a_1 decreases at the downstream region. This is because the turbulence is not maintained near the wall due to the stable thermal stratification.

The variations of vortex structures are shown in Fig. 9. It is discovered that the vortex structure decreases due to the stable thermal stratification in the downstream region in both the cases. In the case of strong stably thermally-stratified turbulent boundary layer, the vortex structure is difficult to observe near the wall in the downstream region due to decrease of turbulence. Figure 10 shows relations of vortex structure and fluctuation of Reynolds shear stresses in y–z plane. The vortex structure is detected by the second invariant velocity gradient tensor, and the green indicates the positive sign of ω_x and the pink shows the negative sign of ω_x. Also, the region purple colored indicates

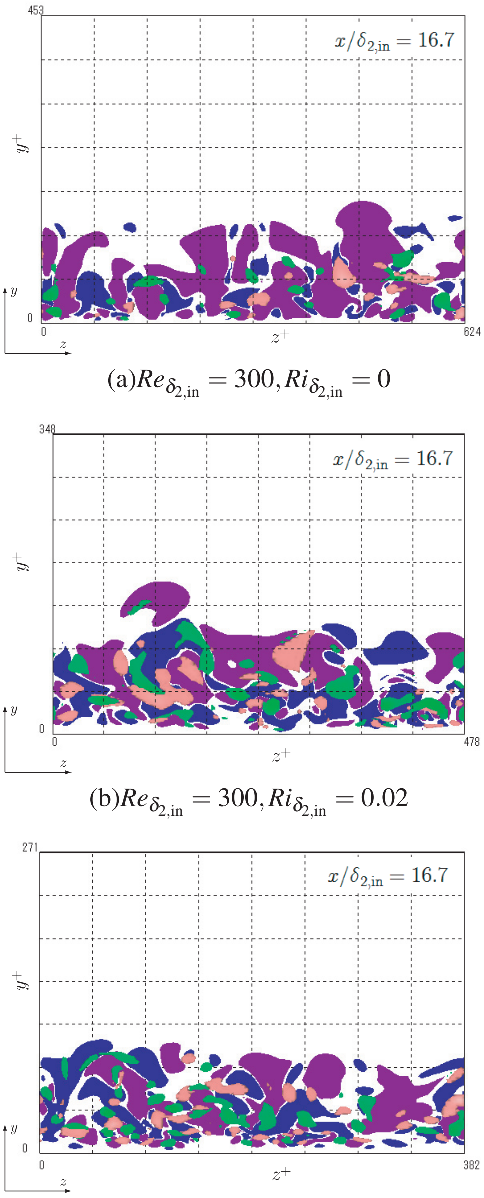

(a)$Re_{\delta_{2,\rm in}} = 300, Ri_{\delta_{2,\rm in}} = 0$

(b)$Re_{\delta_{2,\rm in}} = 300, Ri_{\delta_{2,\rm in}} = 0.02$

(c) $Re_{\delta_{2,\rm in}} = 300, Ri_{\delta_{2,\rm in}} = 0.04$

Figure 10. Relations of vortex structure and fluctuation of Reynolds shear stresses in y–z plane

the positive value of fluctuating uv which is the ejection or sweep motions, and the region blue colored shows the negative value of fluctuating uv which is the interaction motions. For comparison, the case of $Re_{\delta_{2,\rm in}} = 300$ with $Ri_{\delta_{2,\rm in}} = 0$ is included in the figure. In general, the positive value of fluctuating uv distributes around the vortex structure as shown in Fig. 10(a). The negative value of fluctuating uv, however, can be clearly observed more in cases of stable thermal stratification. The negative value of fluctuating uv, however, can be clearly observed more in cases of stable thermal stratification. Therefore, it can be found that the interaction motion apparently contributes the occurrence of CDP.

CONCLUSIONS

DNSs of the stably thermally-stratified turbulent boundary layer have been conducted under various Reynolds and Richardson numbers conditions. In the present DNS, the detailed turbulent statistics of stably thermally-stratified turbulent boundary layer near the wall are clearly indicated in the various conditions. DNS clearly shows the CDP which indicates the negative sign of the Reynolds shear stress and the wall-normal turbulent heat flux with the positive sign of mean velocity and temperature gradients. In the case of strong occurrence of CDP, the local Richardson number always exceeds the critical Richardson number, but the turbulence is maintained. Also, the anisotropy tensor and invariant map are indicated in this paper. It is found that the state of turbulent stress rapidly arrives in the axisymmetric in the case of strong occurrence of CDP. The turbulent heat flux tensor is also shown in order to indicate the variation of thermal field, in which the streamwise turbulent heat flux tensor maintains high value even in the case of strong occurrence of CDP. The relation between the vortex structure and the fluctuation of Reynolds shear stress is shown, where the negative value of fluctuation of Reynolds shear stress frequently appears around the vortex structure in the case of occurrence of CDP.

ACKNOWLEDGEMENT

This research was supported by a Grant-in-Aid for Scientific Research (C), 23560225, from the Japan Society for the Promotion of Science (JSPS).

REFERENCES

Hattori, H., Houra, T. & Nagano, Y. 2007 Direct numerical simulation of stable and unstable turbulent thermal boundary layers. *International Journal of Heat and Fluid Flow* **28**, 1262–1271.

Hattori, H., Houra, T. & Tagawa, M. 2012 Investigations of counter gradient diffusion phenomenon in thermal field of turbulent boundary layer by means of DNS. *Proceedings of the eighth KSME-JSME Thermal and Fluids Engineering Conference, TFEC8* .

Hattori, H & Nagano, Y 2004 Direct Numerical Simulation of Turbulent Heat Transfer in Plane Impinging Jet. *International Journal of Heat and Fluid Flow* **25**, 749–758.

Hattori, H. & Nagano, Y. 2007 Numerical study of turbulent thermal boundary layer under various stable stratifications. *Proceedings of 5th International Symposium on Turbulence and Shear Flow Phenomena* pp. 481–486.

Hattori, H. & Nagano, Y. 2012 Structures and mechanism of heat transfer phenomena in turbulent boundary layer with separation and reattachment via DNS. *International Journal of Heat and Fluid Flow* **37**, 81–92.

Hattori, H., Umehara, T. & Nagano, Y. 2013 Comparative study of DNS, LES and hybrid LES/RANS of turbulent boundary layer with heat transfer over 2D Hill. *Flow, Turbulence and Combustion* **90** (3), 491–510.

Komori, S & Nagata, K 1996 Effects of molecular diffusivities on counter-gradient scalar and momentum transfer in strongly stable stratification. *Journal of Fluid Mechanics* **326**, 205–237.

Ohya, Y. 2001 Wind-tunnel study of atmospheric stable boundary layers over a rough surface. *Boundary-Layer Meteorology* **98**, 57–82.

Simonsen, A J & Krogstad, P.-Å. 2005 Turbulent stress invariant analysis: clarification of existing terminology. *Physics of Fluids* **17**.

Tagawa, M, Fukatsu, M, Nabata, Y & Ohta, Y 2005 Thermal-field structure of a non-premixed turbulent flame formed in a strong pressure-gradient flow. *International Journal of Heat and Fluid Flow* **26**, 905–913.